J. metamorphic Geol., 2008, **26,** 759–774 doi:10.1111/j.1525-1314.2008.00786.x

Formation of clinopyroxene + spinel and amphibole + spinel symplectites in coronitic gabbros from the Sierra de San Luis (Argentina): a key to post-magmatic evolution

G. CRUCIANI,[1] M. FRANCESCHELLI,[1] C. GROPPO,[2] N. BROGIONI[3] AND O. VASELLI[4]
[1]*Dipartimento di Scienze della Terra, Università di Cagliari, Via Trentino 51, 09127, Cagliari, Italy (gcrucian@unica.it)*
[2]*Dipartimento di Scienze Mineralogiche e Petrologiche, Università di Torino, Via Valperga Caluso 35, 10125 Torino, Italy*
[3]*CONICET, Facultad de Ciencias Naturales y Museo, Universidad Nacional de La Plata, Calle 122 & 60, 1900 La Plata, Argentina*
[4]*Dipartimento di Scienze della Terra, Università di Firenze, Via G. La Pira 4, 50121 Florence, Italy*

ABSTRACT The El Arenal metagabbros preserve coronitic shells of orthopyroxene ± Fe-oxide around olivine, as well as three different types of symplectite consisting of amphibole + spinel, clinopyroxene + spinel and, more rarely, orthopyroxene + spinel. The textural features of the metagabbros can be explained by the breakdown of the olivine + plagioclase pair, producing orthopyroxene coronas and clinopyroxene + spinel symplectites, followed by the formation of amphibole + spinel symplectites, reflecting a decrease in temperature and, possibly, an increase in water activity with respect to the previous stage. The metagabbros underwent a complex *P–T* history consisting of an igneous stage followed by cooling in granulite, amphibolite and greenschist facies conditions. Although the *P–T* conditions of emplacement of the igneous protolith are still doubtful, the magmatic assemblage suggests that igneous crystallization occurred at a pressure lower than 6 kbar and at 900–1100 °C. Granulitic *P–T* conditions have been estimated at about 900 °C and 7–8 kbar combining conventional thermobarometry and pseudosection analysis. Pseudosection calculation has also shown that the formation of the amphibole + spinel symplectite could have been favoured by an increase in water activity during the amphibolite stage, as the temperature of formation of this symplectite strongly depends on aH_2O (< 740 °C for $aH_2O = 0.5$; < 790 °C for $aH_2O = 1$). Furthermore, but not pervasive, re-equilibration under greenschist facies *P–T* conditions is documented by retrograde epidote and chlorite. The resulting counterclockwise *P–T* path consists of progressive, nearly isobaric cooling from the igneous stage down to the granulite, amphibolite and greenschist stage.

Key words: coronitic metagabbro; Famatinian orogeny; *P–T* path; reaction history; symplectite.

INTRODUCTION

Symplectite microstructures are common in metamorphic rocks re-equilibrated from granulite and eclogite facies *P–T* conditions. These microstructures always generate great interest as they are invaluable tools in the reconstruction of the metamorphic evolution and *P–T* conditions of the rocks. Although a great number of symplectite types are known from the literature, the majority of mafic rocks contain a single symplectite type, consisting of an intergrowth of two or more metamorphic minerals (mainly Opx, Cpx, Am, Spl; mineral abbreviations according to Kretz, 1983 and Bucher & Frey, 2002). However, when two symplectite types do coexist, their formation has been interpreted in contrasting ways. The coexistence of Am + Spl symplectite and Cpx + Spl symplectite in olivine metagabbros from Mathurapur, Bihar (India) was interpreted by Mall & Sharma (1988) as resulting from the replacement of symplectitic clinopyroxene by pargasitic amphibole.

The coexistence of Px-Spl symplectite and Am-Spl symplectite in mafic rocks from the Buck Creek ultramafic body, North Carolina, and from the Ulten zone, Italy, has been interpreted as resulting either from the single reaction Pl + Ol + H_2O → Cpx + Am + Spl + Opx (Lang *et al.*, 2004) or from a reaction ranging between the two extremes (see Godard & Martin, 2000): (i) Grt + Ol → Opx + Spl + Cpx and (ii) Grt + Ol + H_2O → Opx + Spl + Am, in which the relative abundance of amphibole and clinopyroxene is correlated with local fluctuations of P_{H_2O} (Godard & Martin, 2000).

In the Mafic and Ultramafic Complex of the Sierra de San Luis (Argentina), metagabbros are characterized by the coexistence of Cpx + Spl and Am + Spl symplectites and by corona microstructure at the olivine–plagioclase interface. In this paper, we provide chemical and microstructural data on coronitic metagabbros from El Arenal, Sierra de San Luis, in order to investigate the formation of Cpx + Spl and Am + Spl symplectites in the

context of the metamorphic evolution during the Famatinian orogeny.

GEOLOGICAL SETTING

The central and western sectors of the Sierra de San Luis (Fig. 1a), Eastern Sierras Pampeanas, consist of metasedimentary (mainly migmatites, gneisses, phyllites, micaschists, quartzites), meta-igneous rocks (acidic and mafic to ultramafic) and undeformed plutonic bodies belonging to the Eastern and Western Basement Complex of von Gosen & Prozzi (1998) (broadly equivalent to the Pringles and Nogolí Metamorphic Complexes of Sims *et al*., 1997a). These rocks were formed at the south-western margin of the Gondwana palaeocontinent during the Famatinian orogeny, for which ages spanning from Upper Precambrian to Lower–Middle Palaeozoic have been determined (Pankhurst & Rapela, 1998). A detailed description of the igneous and metamorphic units and structural features of the basement of the Sierra de San Luis can be found in Sato *et al*. (2003, and references therein).

The mafic to ultramafic rocks, grouped in the Mafic–Ultramafic Complex (Malvicini & Brogioni, 1996), later combined into the Las Aguilas Group (Sims *et al*., 1997a,b), and recently included in the El Destino–Las Aguilas Mafic–Ultramafic Belt (Brogioni *et al*., 2007), form a narrow NNE–SSW-trending belt made up of several small lens-shaped bodies along the eastern flank of the Sierra (Fig. 1a). The most conspicuous occurrences of mafic–ultramafic rocks are at Las Aguilas, Virorco and El Fierro, in the southern extreme of the belt, which carry Cu–Ni sulphide mineralization containing platinum-group elements (González Bonorino, 1961; Malvicini & Brogioni, 1996; Mogessie *et al*., 2000; Ferracutti *et al*., 2007; and references therein). The mafic–ultramafic bodies are

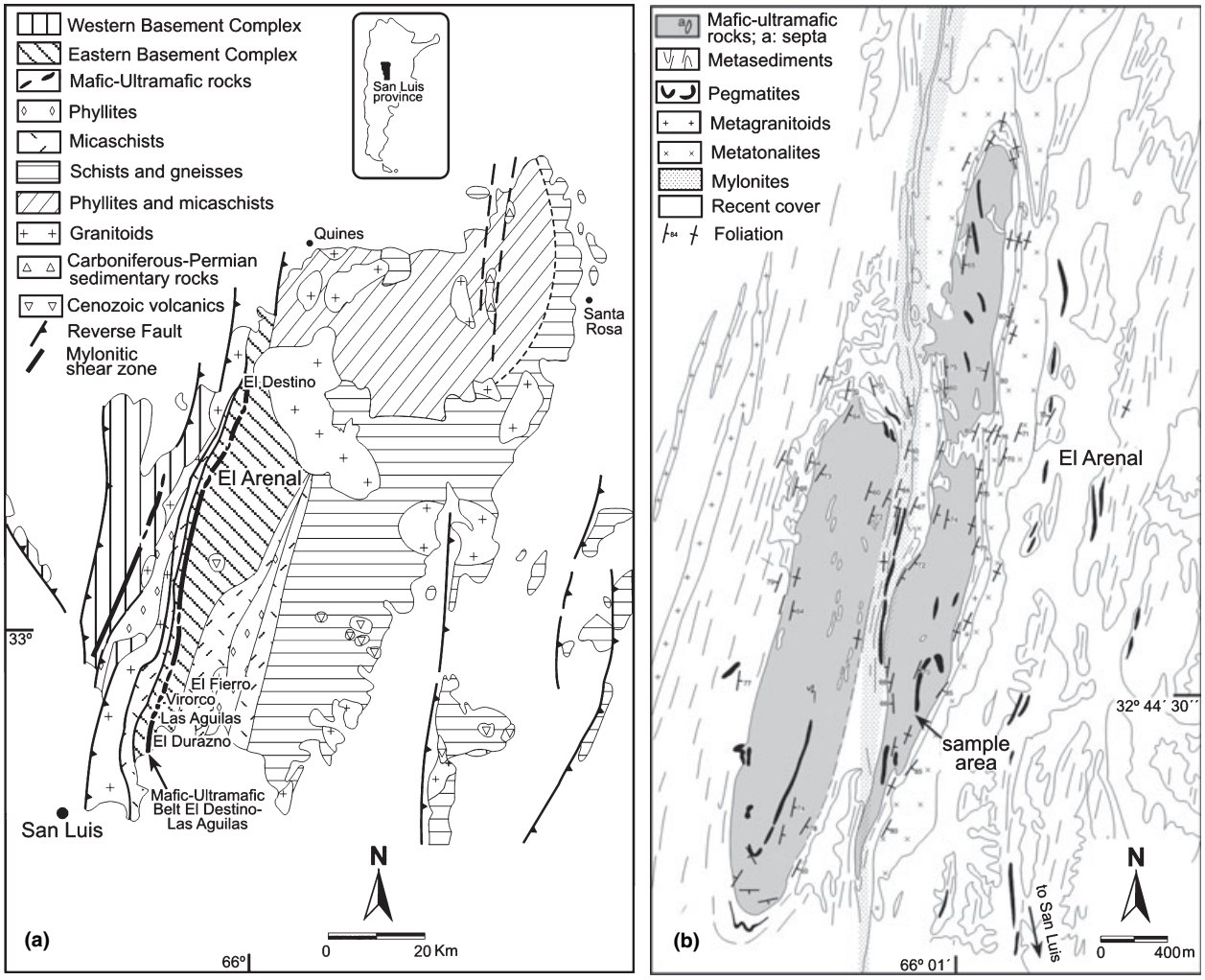

Fig. 1. (a) Geological sketch map of the Sierra de San Luis, Eastern Sierras Pampeanas, modified from Ortiz Suárez *et al*. (1992) and von Gosen & Prozzi (1998); the inset shows the location of the San Luis Province in central Argentina. (b) Geological map of El Arenal mafic bodies, modified from Brogioni (2001).

made up of dark, medium- to coarse-grained metagabbro and minor pyroxenite, hornblendite and dunite (Brogioni, 1994). At Virorco, some lenses display coarse-grained ultramafic rocks in the core and more fine-grained mafic rocks in the outer part. In the same area, pyroxenite cumulates alternate with melagabbros in the lens core (Brogioni, 2001). Most mafic and ultramafic bodies were affected by folding, stretching and shearing, and display some kind of metamorphic foliation and/or lineation parallel to the main NNE–SSW foliation of the metasedimentary country rocks. According to Brogioni *et al.* (2007 and references therein), the rocks from the Mafic Ultramafic Belt are derived from Ti-poor, olivine-rich tholeiitic magmas emplaced in an extensional back-arc regime or a marginal basin. Mafic magmatism, as indicated by an U–Pb zircon age obtained for a felsic segregation from Las Aguilas (Sims *et al.*, 1997a,b, 1998), occurred at 478 ± 6 Ma, in the Early Ordovician, before the Famatinian orogenic deformation (Brogioni, 2001; Brogioni *et al.*, 2007).

The studied samples are coronitic metagabbros (coronitic melagabbronorites according to Brogioni *et al.*, 2007) coming from a pair of lenses about 2 km in length and 400 m in width in the northern part of the Mafic–Ultramafic Complex of El Arenal (Fig. 1b). The samples are dark-coloured, fine- to coarse-grained metagabbros showing a variable amphibole content. Coronitic metagabbros are characterized by: 42–45 wt% SiO_2, 0.18–0.29 wt% TiO_2, 13.16–17.63 wt% Fe_2O_{3tot}, 4.53–8.56 wt% CaO, 0.57–0.75 wt% Na_2O and 0.15–0.31 wt% K_2O. Al_2O_3 is mostly between 6.96 and 9.11 wt%. The high MgO content, variable between 16 and 25 wt%, suggests a cumulate origin. On the basis of CIPW Norm, the metagabbros are olivine (up to ~44 wt%)–hypersthene (up to ~32 wt%) normative (Brogioni *et al.*, 2007). Country rocks are coarse-grained, mostly migmatitic Bt-Qtz-feldspathic gneisses and minor quartzite layers, affected by shear deformation which led to the development of mylonites close to the margins of the mafic lenses.

PETROGRAPHY

The El Arenal coronitic metagabbros retain relics of an igneous assemblage (Fig. 2a–c) dominated by plagioclase (Pl_0), olivine (Ol_0), orthopyroxene (Opx_0), spinel (Spl_0) and minor phlogopite (Phl_0). Highly cracked igneous olivine, up to a few millimetres in size, displays embayments at the edges and includes small rounded Fe-oxides, Fe–Cr oxide, and pyrite of variable size and shape (Figs 2a & 3a). Pl_0 occurs as single grains of 5–6 mm in size or in medium-grained crystals characterized by the growth of strongly oriented amphibole, clinopyroxene and orthopyroxene microcrystals up to 0.5 mm in length (Fig. 2b,d). K-feldspar grown on igneous plagioclase has also been observed. Microstructural observation suggests that K-feldspar predates the formation of small oriented amphibole, clinopyroxene and orthopyroxene microcrystals growing on Pl_0 (Fig. 3f). Incipient replacement by epidote (Fig. 2a) and calcite occurs at the rim of plagioclase crystals. Igneous orthopyroxene (Opx_0) contains oriented trails of Fe-oxide and consists of grains up to 3 mm in size (Fig. 2c). A sporadic growth of plagioclase (Pl_1) along the fractures of orthopyroxene is unevenly observed. Submillimetric grains of igneous spinel (Spl_0) also show oriented inclusions of Fe-oxide. Fe–Cr oxide is occasionally preserved in the spinel core, whereas scattered ankerite grains up to a few tens of microns overgrow spinel. Phlogopite occurs in a few samples as randomly oriented flakes up to 1–1.5 mm in length, and is partially replaced by coarse-grained amphibole.

The most impressive textural feature of the El Arenal coronitic metagabbros consists of well-preserved coronitic shells (Figs 2a & 3a) of orthopyroxene ± Fe-oxide between olivine and plagioclase, in a variety of associations with Cpx + Spl or Am + Spl symplectites. Three main types of corona can be distinguished: (i) the most common coronas are made up of a regular, continuous layer of orthopyroxene (Opx_1) around olivine, surrounded by a Cpx + Spl and/or Am + Spl symplectite matrix (Fig. 2a); (ii) some coronas around olivine consist of an orthopyroxene layer associated with subordinate, scattered blebs of Fe-oxide up to a few tens of microns in size (Fig. 3a); and (iii) in the most re-equilibrated samples, the coronitic assemblage consists of rounded to slightly elongated clusters of polygonal orthopyroxene, preserving scattered relics of olivine in their inner part and mostly surrounded by a Am + Spl symplectite matrix (Fig. 2d).

Two types of symplectite with different mineral abundance and grain size can be recognized: (i) Cpx_1 + Spl_1 symplectite and (ii) Am_1 + Spl_2 symplectite (Figs 2a,b,d & 3b–e). An additional, but very rare, Opx_1 + Spl_1 symplectite can sometimes be found at the outer margins (those facing anorthite) of Opx_1 (Fig. 3f). The Cpx_1 + Spl_1 symplectite (Figs 2a,b & 3b–d) consists of a fine-grained, worm-shaped microstructure of clinopyroxene with randomly oriented lamellae of green spinel. This symplectite commonly occurs as a discontinuous shell, up to a few millimetres in thickness, between Opx_1 on one side and Pl_0 on the other. In some selected Cpx_1 + Spl_1 microdomains, the proportions of clinopyroxene and spinel in the symplectite have been estimated by image analysis. Although their proportions in the symplectite vary, their relative abundance usually ranges between 70% and 80% clinopyroxene and between 20% and 30% spinel.

In some microdomains it is possible to observe the following complete sequence of layers between igneous olivine and plagioclase:

$$Ol_0 \rightarrow Opx_1 (\text{or } Opx_1 + Spl_1 \text{symplectite}) \rightarrow Cpx_1 + Spl_1 \text{symplectite} \rightarrow Pl_0$$

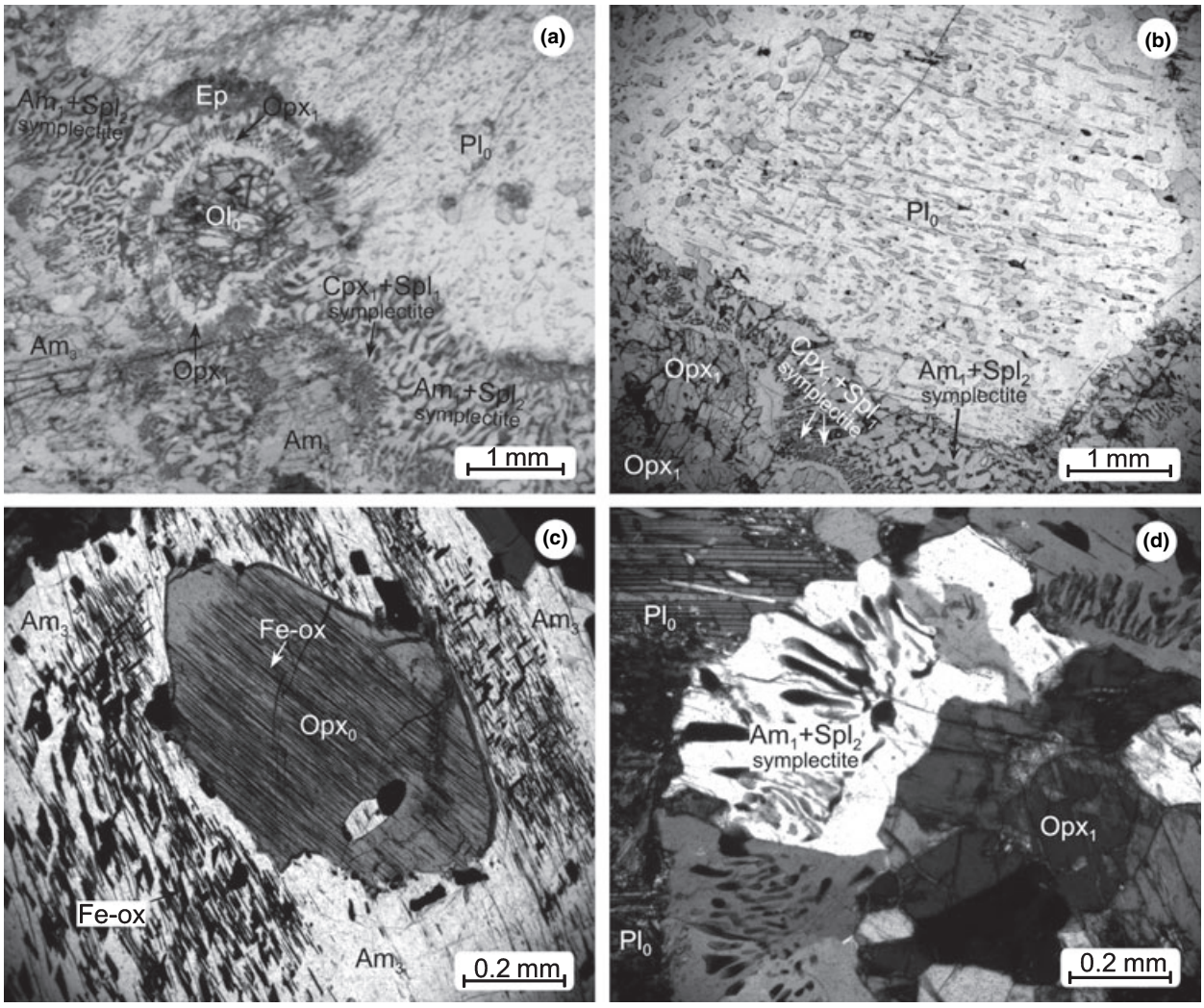

Fig. 2. Microphotographs showing the main microstructural features of the El Arenal metagabbro. (a) Orthopyroxene corona and symplectite matrix separating igneous olivine from plagioclase (sample NB11); note, to the upper left, epidote (Ep) growth at the plagioclase–symplectite interface; one polar (b) Igneous plagioclase (Pl_0), surrounded by Cpx_1 + Spl_1 and Am_1 + Spl_2 symplectites. Note the overgrowth on Pl_0 of oriented small crystals of orthopyroxene, amphibole and spinel (sample NB6); one polar; (c) Igneous orthopyroxene (Opx_0) with trails of Fe-oxide, preserved within the core of an amphibole porphyroblast (Am_3) (sample NB3); crossed polars; (d): Am_1 + Spl_2 symplectites at the interface between igneous plagioclase (Pl_0) and orthopyroxene (Opx_1) clusters replacing olivine (sample NB11); crossed polars.

The Am_1 + Spl_2 symplectite (Figs 2a,b,d & 3b–e) is by far the most abundant in the coronitic metagabbros from El Arenal. It consists of an intergrowth of abundant pale-green amphibole and subordinate micron-sized droplets and lamellae of green spinel. When the Cpx_1 + Spl_1 symplectite is scarce or almost absent, the Am_1 + Spl_2 symplectite is localized between Opx_1 and Pl_0 (Figs 2d & 3d). In this case, spinel abundance strongly decreases, and the Am_1 + Spl_2 symplectite smoothly changes into a spinel-free layer of amphibole a few microns in thickness with a thin tremolite layer (Am_2) in immediate contact with Opx_1 (Fig. 3e). A thin tremolite layer has also been found between Cpx_1 and Opx_1 (Fig. 3e). The Am_1 + Spl_2 symplectite is poorer in spinel compared with the Cpx_1 + Spl_1 symplectite. Image analysis revealed that 80–85% of the symplectite consists of amphibole, whereas the remaining 15–20% is made up of spinel.

The Cpx_1 + Spl_1 and Am_1 + Spl_2 symplectites are often in contact and, although the boundary between them is usually sharp, they sometimes show interfingering relationships. The size, shape and orientation of the spinel lamellae varies greatly in the two symplectites types (Fig. 2a,b): in the Cpx_1 + Spl_1 symplectites the spinel lamellae are very fine-grained and do not show any particular orientation, while spinel lamellae in the Am_1 + Spl_2 symplectite are more coarse-grained with a well-defined orientation, commonly radiating from the coronitic assemblage (Fig. 2a,d). When the two

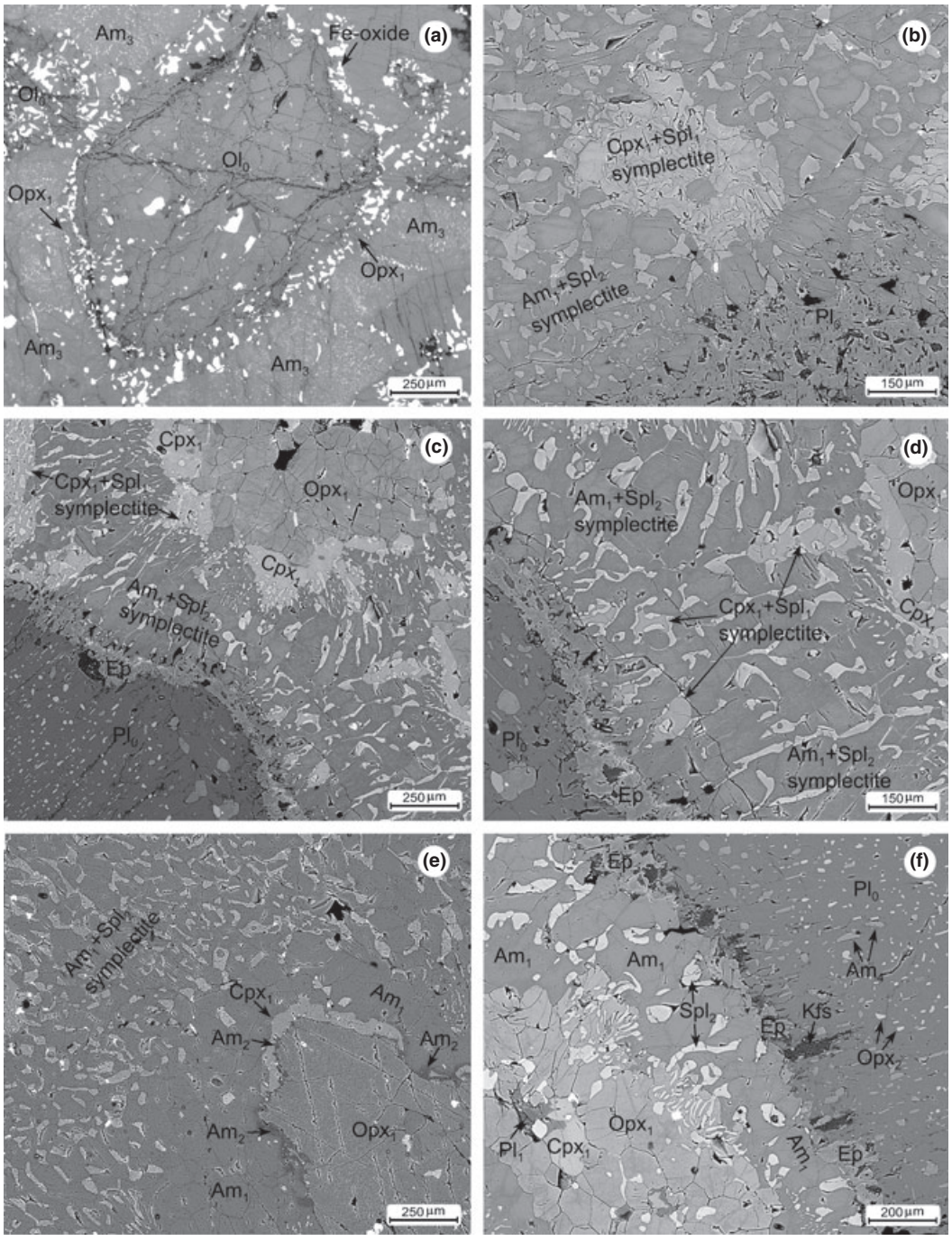

Fig. 3. BSE images of the El Arenal coronitic metagabbro. (a): Igneous olivine (Ol_0) with a well developed Opx_1 + Fe-oxide corona is enclosed within an amphibole porphyroblast (Am_3) (sample NB6); (b): Patch of Cpx_1 + Spl_1 symplectite within the Am_1 + Spl_2 symplectite (sample NB6); (c): Relationships between the Cpx_1 + Spl_1 symplectite and the Am_1 + Spl_2 symplectite at the interface between igneous plagioclase (Pl_0) and an orthopyroxene cluster (Opx_1) (sample NB6); (d): Detail of Fig. 3c, showing three patches of Cpx_1 + Spl_1 symplectite within the Am_1 + Spl_2 symplectite; (e): Gradual transition between Am_1 + Spl_2 symplectite and a spinel-free layer of amphibole in contact with orthopyroxene. Worthy of note is the tremolitic layer (Am_2) at the boundary between amphibole and orthopyroxene (sample NB1); (f): Spinel lamellae in coronitic orthopyroxene (Opx_1 + Spl_1 symplectite) at the interface between igneous plagioclase (Pl_0) and an orthopyroxene cluster (sample NB6); strongly oriented amphibole (Am_4) and orthopyroxene (Opx_2) microcrystals grow on igneous plagioclase and K-feldspar. Note to the right a discontinuous epidote layer at the plagioclase-symplectite interface.

symplectites are in contact, a careful observation at their transition zone reveals that orientation of the spinel lamellae does not significantly vary, and that spinel lamellae originating from one symplectite often continues into the other adjacent symplectite (Fig. 3b–d). Often, the Cpx_1 + Spl_1 and Am_1 + Spl_2 symplectites appear to be unevenly distributed resembling a patchy microstructure in which scattered patches of the Cpx_1 + Spl_1 symplectite are surrounded by the Am_1 + Spl_2 symplectite (Fig. 3b–d).

Pale-green amphibole (Am_3) growing on relict igneous orthopyroxene (Opx_0) and olivine (Ol_0), commonly develops into recognizable porphyroblasts (Figs 2c & 3a). Where the replacement of orthopyroxene has been complete, the core of the amphibole porphyroblasts preserves oriented trails of Fe-oxide of the previous pyroxene. In other cases, relics of orthopyroxene and olivine are preserved within the amphibole porphyroblast. Within their core, amphibole porphyroblasts sometimes preserve olivine grains with their coronitic shell (Fig. 3a) and/or symplectitic microstructures. Dolomite growth along the fractures of coarse-grained amphibole has sometimes been observed.

MINERAL CHEMISTRY

Chemical compositions of relict igneous minerals, coronitic and symplectitic minerals and other metamorphic minerals were determined with a fully automated Cameca SX50 electron microprobe at the University of Firenze, Italy. Operating conditions were 20 kV accelerating voltage and 20 nA sample current, with a diameter beam ~1 μm. Back-scattered electron (BSE) imaging, X-ray mapping and additional EDS analyses were performed with a SEM FEI Quanta 200 at the University of Cagliari, Italy. Selected electron microprobe analyses of relict igneous minerals, coronitic minerals, symplectite minerals and other minerals from the metagabbros from El Arenal are reported in Table 1.

Igneous olivine (Ol_0) has a fairly homogeneous composition (Fo = 79–85 mol.%) with negligible Mn content (up to 0.006–0.007 a.p.f.u.). Anorthite content of igneous plagioclase (Pl_0) is greater than 95 mol.%. No significant compositional variation has been observed between cores and rims. Metamorphic plagioclase (Pl_1) that grew along fractures in orthopyroxene, as well as in the rock matrix, is oligoclase ($An_{\sim 24}$).

Clinopyroxene Cpx_1, forming a worm-like symplectite with spinel, is diopside with X_{Mg} = 0.85–0.88. Ca is in the range 0.91–0.93 a.p.f.u. and the maximum Na content is 0.006 a.p.f.u. Orthopyroxene analyses from Table 1 include igneous orthopyroxene (Opx_0) with oriented trails of Fe-oxide, as well as coronitic orthopyroxene (Opx_1) around olivine. All compositions plot on the Mg-rich side of the enstatite–ferrosilite join. Ti and Cr contents are negligible and Al_{tot} ranges between 0.09 and 0.14 a.p.f.u. Opx_0 is enstatite-rich ($X_{Mg} \sim 0.80$), with no significant differences between core and rim. Opx_1 has a fairly constant composition (En = 0.80–0.81 mol.%). Micron-sized orthopyroxene (Opx_2) crystals growing on Pl_0 show a similar composition with a slightly lower X_{Mg} ratio (0.73–0.75) compared with the other groups.

Amphibole is calcic according to the classification of Leake *et al.* (1997). Amphibole from the symplectite (Am_1) ranges in composition from Mg-hornblende to tschermakite. Am_2 is tremolite with X_{Mg} = 0.89 and Al_{tot} up to 0.6 a.p.f.u. Amphibole porphyroblasts (Am_3) are Mg-hornblende to tschermakite with X_{Mg} = 0.80. The core of these porphyroblasts sometimes shows a slight enrichment in Na_2O and Cr_2O_3, when compared with the rim. Micron-sized amphibole (Am_4) growing on Pl_0 has the same composition as Am_3.

Spinel belongs to the spinel–hercynite series. Igneous spinel (Spl_0), sometimes associated with coronitic orthopyroxene (Opx_1), is Cr-rich (up to 1.5 wt% of Cr_2O_3) and depleted in Al compared with the spinel from symplectites. No systematic compositional differences have been observed between symplectitic spinel associated with clinopyroxene (Spl_1) and that associated with amphibole (Spl_2). X_{Mg} of phlogopite is in the range 0.89–0.92. Al^{IV} is ~2.1, Al^{VI} ~1.1 and K is up to 1.7 a.p.f.u. Mn and Cr contents are negligible. Epidote belongs to the clinozoisite–epidote series. Fe^{3+} content is ~0.03 a.p.f.u.

REACTION HISTORY AND MINERALOGICAL RE-EQUILIBRATION

Microstructural features in the El Arenal coronitic metagabbros reflect a complex metamorphic history, summarized in the following stages.

Igneous stage – This stage is documented by relics of igneous phases (mainly olivine, orthopyroxene, anorthite, phlogopite, Cr-rich spinel, opaque minerals and pyrite) surrounded by coronitic microstructures or preserved as inclusions in amphibole porphyroblasts. The occurrence of oriented trails of Fe-oxide in the core of igneous orthopyroxene suggests that they were exsolved during cooling after magmatic crystallization. K-feldspar, growing on igneous plagioclase and pre-dating the formation of small oriented metamorphic amphibole and pyroxene microcrystals, may be a late magmatic phase.

Pyroxene–spinel symplectite stage – This stage is documented by the formation of coronitic orthopyroxene and Cpx_1 + Spl_1 symplectites derived from the breakdown of the Ol_0 + Pl_0 pair. The distribution and sequence of coronitic minerals are controlled by Al and Ca diffusion rates, as phases with higher Al (i.e. spinel) and Ca contents (i.e. clinopyroxene) preferentially formed at the plagioclase side, whereas the Al- and Ca-poorer phase (i.e. orthopyroxene) grew in contact with olivine.

Table 1. Representative analyses of igneous, coronitic, symplectitic, and other minerals from sample NB1 and NB6 of the metagabbro of El Arenal.

	Relict igneous minerals								
Mineral	Ol_0	Ol_0	Pl_0	Pl_0	Spl_0	Spl_0	Opx_0	Opx_0	Phl_0
Sample	NB6	NB1	NB6	NB1	NB6	NB1	NB6	NB1	NB6
SiO_2	40.05	39.60	43.72	43.99	–	–	55.05	55.20	40.16
TiO_2	–	–	–	–	–	–	–	0.02	0.71
Al_2O_3	–	–	36.70	35.59	62.11	63.94	3.05	3.15	17.74
Cr_2O_3	–	–	–	–	0.90	1.10	0.01	0.02	0.02
FeO_{tot}	15.70	19.14	0.05	0.03	20.99	19.10	13.02	12.50	5.25
MnO	0.20	0.26	–	–	–	0.10	0.30	0.24	0.01
MgO	45.00	41.70	–	–	16.00	16.70	29.57	29.50	23.17
CaO	–	–	20.02	20.07	–	–	0.25	0.20	–
Na_2O	–	–	0.15	0.31	–	–	–	–	0.50
K_2O	–	–	–	–	–	–	–	–	9.53
Total	100.95	100.70	100.64	99.99	100.00	100.94	101.25	100.83	97.09
Oxy	4	4	8	8	4	4	6	6	22
Si	1.01	1.01	2.01	2.04	–	–	1.93	1.94	5.58
Al_{tot}	–	–	1.99	1.94	1.92	1.94	0.13	0.13	2.91
Ti	–	–	–	–	–	–	–	0.00	0.07
Cr	–	–	–	–	0.02	0.02	–	0.00	0.00
Fe^{2+}	0.37	0.41	0.00	0.00	0.46	0.41	0.38	0.37	0.61
Fe^{3+}	–	–	–	–	–	–	–	–	–
Mn	0.01	0.01	–	–	–	0.00	0.01	0.01	0.00
Mg	1.61	1.58	–	–	0.63	0.64	1.55	1.54	4.80
Ca	–	–	0.99	1.00	–	–	0.01	0.01	–
Na	–	–	0.01	0.03	–	–	–	–	0.14
K	–	–	–	–	–	–	–	–	1.69
X_{Mg}	0.81	0.80	–	–	0.58	0.61	0.80	0.81	0.89

	Corona minerals		Symplectite minerals							Other metamorphic minerals			
Mineral	Opx_1	Opx_1	Cpx_1	Cpx_1	Am_1	Am_1	Spl_1	Spl_1	Spl_2	Am_2	Am_3	Pl_1	Ep
Sample	NB6	NB1	NB6	NB1	NB6	NB1	NB6	NB1	NB6	NB6	NB6	NB6	NB6
SiO_2	55.18	55.33	53.42	53.83	47.92	46.18	–	–	–	55.72	45.35	62.68	39.81
TiO_2	–	–	0.06	0.04	0.07	0.33	–	–	–	–	0.14	–	0.01
Al_2O_3	3.08	2.89	2.47	3.01	11.72	13.60	65.10	65.20	64.19	3.65	12.84	23.28	33.56
Cr_2O_3	–	–	–	–	0.05	0.08	0.30	0.01	0.25	–	0.13	–	–
FeO_{tot}	12.70	12.40	4.73	4.48	7.20	7.45	19.80	19.52	19.34	4.63	7.89	–	0.49
MnO	0.25	0.29	0.11	0.08	0.07	0.08	0.10	0.14	0.08	–	0.14	–	–
MgO	29.38	29.81	15.80	15.79	17.51	16.71	15.55	15.60	16.48	21.19	17.68	–	–
CaO	0.31	0.25	23.85	23.67	12.65	12.50	–	–	–	12.00	11.54	5.03	23.86
Na_2O	–	–	0.08	0.09	1.58	1.75	–	–	–	0.56	1.74	9.01	0.16
K_2O	–	–	–	–	0.18	0.47	–	–	–	–	0.40	–	–
Total	100.90	100.97	100.52	100.99	98.95	99.15	100.85	100.47	100.34	97.75	97.85	100.00	97.89
Oxy	6	6	6	6	23	23	4	4	4	23	23	8	12.5
Si	1.94	1.94	1.95	1.95	6.72	6.49	–	–	–	7.69	6.47	2.78	3.01
Al_{tot}	0.13	0.12	0.11	0.13	1.94	2.25	1.98	1.98	1.96	0.59	2.16	1.22	2.99
Ti	–	–	0.00	0.00	0.01	0.04	–	–	–	–	0.02	–	0.00
Cr	–	–	–	–	0.01	0.01	0.01	–	0.01	–	0.02	–	–
Fe^{2+}	0.37	0.36	0.14	0.14	0.84	0.88	0.43	0.42	0.42	0.53	0.94	–	–
Fe^{3+}	–	–	–	–	–	–	–	–	–	–	–	–	0.03
Mn	0.01	0.01	0.00	0.00	0.01	0.01	0.00	0.00	0.00	–	0.02	–	–
Mg	1.54	1.56	0.86	0.85	3.66	3.50	0.60	0.60	0.64	4.36	3.76	–	–
Ca	0.01	0.01	0.93	0.92	1.90	1.88	–	–	–	1.77	1.77	0.24	1.93
Na	–	–	0.01	0.01	0.43	0.48	–	–	–	0.15	0.48	0.77	0.02
K	–	–	–	–	0.03	0.08	–	–	–	–	0.07	–	–
X_{Mg}	0.80	0.81	0.86	0.86	0.81	0.80	0.58	0.59	0.60	0.89	0.80	–	–

As shown above, some coronas around olivine consist of an orthopyroxene layer associated with subordinate, scattered blebs of Fe-oxide. Their formation, localized into particular microdomains, was probably controlled by the diffusion and initial distribution of Fe. In those microdomains in which Fe-oxides occur in the corona, it is likely that Fe failed to diffuse from olivine to the symplectite matrix and its concentration within the orthopyroxene corona resulted in the growth of scattered blebs of Fe-oxide. The resulting mineralogical assemblage at this stage consisted of olivine and plagioclase relics + orthopyroxene + clinopyroxene + spinel + phlogopite + opaque minerals + sulphides. The coexistence of orthopyroxene and clinopyroxene suggests re-equilibration under granulite facies *P–T* conditions.

Amphibole–spinel symplectite stage – This stage is dominated by the formation of the $Am_1 + Spl_2$ symplectite around the coronitic microdomains and also by the development of amphibole porphyroblasts (Am_3) in the matrix and on granoblastic orthopyroxene (Opx_0). The occurrence of scattered relics and patches of $Cpx_1 + Spl_1$ symplectite within the $Am_1 + Spl_2$ symplectite, as well as the interfingering relationships at the boundary between the two symplectite types, implies that the $Am_1 + Spl_2$ symplectite formed later than the $Cpx_1 + Spl_1$ symplectite. The occurrence of Pl_1 that has grown along the edges and within the fractures of Opx_0, and sporadically within the matrix, should also be related to this stage. The widespread growth of amphibole, which suggests a pervasive hydration of the rocks after the granulite stage, is also worthy of note.

Late stage – The last stage of metamorphism led to the development of fine-grained retrograde minerals such as chlorite, muscovite, dolomite, ankerite and calcite that have grown on minerals of the previous stages. The formation of dolomite at the expense of phlogopite and the overgrowth of epidote on igneous plagioclase can also be related to this stage.

MODELLING OF CORONA- AND SYMPLECTITE-FORMING REACTIONS

In order to interpret the metamorphic evolution of the El Arenal coronitic metagabbros, the microstructural data are combined with quantitative balancing of metamorphic reactions by the 'least-squares' method using CSpace (Torres-Roldan *et al.*, 2000). The mineral compositions (in oxide molar percentage) of the main phases in the coronitic metagabbros represent the input data, irrespective of whether they are reactants or products. A successful reaction should be consistent with the observed microstructures (i.e. inferred reactants and products should appear on opposite sides of the model reaction) and the stoichiometric coefficients of the reaction should be in agreement with the observed amounts of mineral products. The accuracy of the results can be appreciated from the matrix of residuals (Model – Input) reported in the Appendix.

Including olivine (Ol_0), anorthite (Pl_0), coronitic orthopyroxene (Opx_1), symplectitic clinopyroxene (Cpx_1) and symplectitic spinel (Spl_1) from sample NB6 (mineral compositions in Table 1) in the calculation, CSpace rapidly converged on the following reaction, which accounts for the formation of orthopyroxene coronas around olivine and $Cpx_1 + Spl_1$ symplectites at the Ol_0–Pl_0 interface:

$$1Pl_0 + 1.82Ol_0 \rightarrow 0.94Opx_1 + 1.05Cpx_1 + 0.88Spl_1 \quad (1a)$$

Reaction (1a) is consistent with the observed microstructure in that olivine (Ol_0) and plagioclase (Pl_0) are reactants and coronitic and symplectitic minerals (Opx_1, Cpx_1, Spl_1) are products. Residuals (see the Appendix) are usually low, except for Fe (measured Fe = 0.002; modelled Fe = 0.308) which is outside analytical error in plagioclase. However, the relatively high residuals for Fe in plagioclase, already pointed out by Fisher (1989) and Lang *et al.* (2004), may result from small analytical errors or from incomplete Fe equilibration between plagioclase and other minerals. Reaction (1a) is supported by the relative volumes of the reactants and products calculated from the stoichiometric coefficients and tabulated molar volumes available from the literature (Helgeson *et al.*, 1978). According to the calculation reported in Table 2, reaction (1a) would have resulted in a $Cpx_1 + Spl_1$ symplectite consisting of 67% clinopyroxene and 33% spinel, which is similar to the proportion estimated by image analysis in selected microdomains of the $Cpx_1 + Spl_1$ symplectite in sample NB6 (Cpx = 70–82%, Spl = 18–30%). Reaction (1a) is also in agreement with modal proportions of coronitic orthopyroxene (Opx_1), which is usually subordinate in comparison with symplectitic clinopyroxene (Cpx_1). A small amount of the orthopyroxene generated by reaction (1a) should also have contributed to the development of the $Opx_1 + Spl_1$ symplectite locally observed in a few microdomains.

The introduction of H_2O during the breakdown of the $Pl_0 + Ol_0$ pair may produce the $Am_1 + Spl_2$ symplectites according to the following reaction:

$$1Pl_0 + 1.39Ol_0 + 0.52H_2O \rightarrow 0.51Am_1 + 0.51Spl_2 \quad (1b)$$

Reaction (1b) produces 87% amphibole and 13% spinel (see Table 2), i.e. relative proportion very similar to those estimated by image analyses in $Am_1 + Spl_2$ symplectite microdomains of sample NB6 (Am = 71–85%, Spl = 15–29%). Residuals from reaction (1b) are comparable with those of reaction (1a), except for Na residuals, which are generally higher for reaction (1b) when compared with reaction (1a). This is probably due to Na being slightly mobile or from Na-bearing phases that slightly evolved in composition during the $Am_1 + Spl_2$ symplectite formation. A linear combination between reactions (1a) and (1b) gives a reaction similar to that proposed by Lang *et al.* (2004) for the contemporaneous formation of Am + Spl and Cpx + Spl symplectites in the rocks from Buck Creek California. However, the microstructural features discussed above (patches of $Cpx_1 + Spl_1$ symplectite within the $Am_1 + Spl_2$ symplectite; interfingering relationships between the two symplectites, orientation of spinel lamellae at the transitions from one symplectite to another, etc.) imply that, at least in some cases, the $Am_1 + Spl_2$ symplectite grows after the $Cpx_1 + Spl_1$ symplectite, leading us to reject the hypothesis that all the $Am_1 + Spl_2$ and $Cpx_1 + Spl_1$ symplectites in the El Arenal metagabbros formed simultaneously.

Table 2. (a) Volumes of reactants and products in reactions (1a), (1b) and (2), calculated from coefficients of the balanced reactions and from molar volumes (molar volumes for olivine, plagioclase, orthopyroxene, clinopyroxene, amphibole, and spinel are from Helgeson *et al.*, 1978; molar volume for H_2O at 800 °C and 8 kbar is from Burnham *et al.*, 1969). (b) Abundance of clinopyroxene, spinel and amphibole in some selected symplectite microdomains from sample NB6. Microdomains 1–5 refer to the Cpx_1 + Spl_1 symplectite; microdomains 6–10 refer to the Am_1 + Spl_2 symplectite.

	Reactants					Products				
	Pl	Ol	Opx	H_2O	sum	Cpx	Am	Spl	Opx	sum
(a)										
V (cm^3/m)	100.79	43.79	62.56	21.99		66.09	272.92	39.71	62.56	
Reaction (1a)	1.00	1.82				1.05		0.88	0.94	
Volume (cm^3)	100.79	79.70			180.49	69.39		34.94	58.81	163.15
%Volume	56	44				43		21	36	
$\%Volume_{sympl}$						67		33		
Reaction (1b)	1.00	1.39		0.52			0.51	0.51		
Volume (cm^3)	100.79	60.87		11.43	173.09		139.19	20.25		159.44
%Volume	58	35		7			87	13		
$\%Volume_{sympl}$							87	13		
Reaction (2)	1.00		1.96	0.91			0.83	0.29		
Volume (cm^3)	100.79		122.62	20.01	243.42		226.52	11.52		238.04
%Volume	41		50	8			95	5		
$\%Volume_{sympl}$							95	5		
(b)										
Microdomain	1	2	3	4	5	6	7	8	9	10
Cpx	80	82	70	74	77					
Am						72	71	80	85	82
Spl	20	18	30	26	23	28	29	20	15	18

As already observed by Godard & Martin (2000), the kelyphite-forming reaction in garnet peridotites from the Ulten Zone ranges between the two extreme reactions: (i) Grt + Ol → Opx + Spl + Cpx and (ii) Grt + Ol + H_2O → Opx + Spl + Am, and the relative abundance of amphibole and pyroxene is correlated with local fluctuations of P_{H_2O}. In the El Arenal coronitic metagabbros two diachronous reactions, such as (1a) and (1b), are needed to explain the formation of the Cpx_1 + Spl_1 and Am_1 + Spl_2 symplectites. It is likely that Cpx_1 + Spl_1 symplectites mainly formed during an anhydrous granulite stage, pre-dating the formation of Am_1 + Spl_2 symplectites during a hydrous stage.

Although reaction (1b) could explain the modal abundances of amphibole and spinel in the symplectites microdomains, it does not account for the pervasive growth of amphibole on orthopyroxene. We propose that reaction (1b) operated locally in combination with the following reaction, which better accounts for the orthopyroxene replacement by amphibole porphyroblasts:

$$1Pl_0 + 1.96Opx_0(\text{or } Opx_1) + 0.91H_2O \rightarrow 0.83Am + 0.29Spl_2 \quad (2)$$

The higher Am/Spl_2 coefficient ratio of reaction (2), when compared with reaction (1b), implies higher amphibole content near to 95% of the total amount of reaction products (see Table 2). Of amphibole produced by reaction (2), an amount of about 20% could form the symplectite together with spinel (Am_1), while the remaining replaces orthopyroxene or grew in the matrix as amphibole porphyroblasts (Am_3).

However, not all the observed microstructures can exhaustively be explained with the reactions proposed above. An additional explanation should be invoked to account for the local formation of tremolite at the rim of the spinel-free layer of amphibole in contact with coronitic orthopyroxene. Tremolite occurrence in the studied rocks can be compared with that described by Ikeda *et al.* (2007) in the coronitic meta-ultramafic rocks from Sefuri Mountains, NW Kyushu, Japan. These authors recognized reaction rims at the olivine–plagioclase interface consisting of an Am–Spl symplectite on the plagioclase side (symplectite zone) and calcic amphibole (with a systematic decrease in Al content and an increase in Mg/Mg + Fe with decreasing distance from olivine) at the olivine side (tremolite zone). The similar occurrence in our samples of Al-rich, Mg-poor amphibole (hornblende) in the symplectite domain and of Al-poor, Mg-rich tremolite rim in contact with coronitic orthopyroxene suggests that the two zones developed at the expense of plagioclase and olivine, respectively, and that Al was approximately immobile during symplectite formation. The formation of tremolite in the rocks from Sefuri Mountains has been explained with an open-system reaction in which tremolite forms from the destabilization of olivine + plagioclase pair (see reaction 12 in Ikeda *et al.*, 2007, p. 303). However, in our rocks, a similar reaction would have resulted in a tremolite-bearing symplectite, which has never been observed. The lack of tremolitic amphibole in the symplectite and the development of tremolite mainly at the contact between coronitic orthopyroxene and symplectitic clinopyroxene (Fig. 3e) can be better explained with a reaction that involves coronitic orthopyroxene and

symplectitic clinopyroxene as possible reactants. Therefore, according to the textural occurrence, we believe that the tremolite layer in the coronitic metagabbros from El Arenal should derive from the destabilization of the Opx_1–Cpx_1 pair with the contribution of a fluid phase according to the reaction:

$$1Cpx_1 + 0.82Opx_1 + 0.49H_2O \rightarrow 0.47Am_2 \quad (3)$$

The tremolitic layer locally surrounding coronitic orthopyroxene thus does not represent a product of a late metamorphic re-equilibration, but results from a local hydration of the anhydrous corona assemblage.

P–T PSEUDOSECTIONS

The reaction sequence experienced by the El Arenal coronitic metagabbros and the formation of the Cpx_1 + Spl_1 and Am_1 + Spl_2 symplectites can be modelled by using *P–T* pseudosection calculations. As coronitic and symplectitic microstructures represent local equilibrium at the microdomain scale, the composition of the whole-rock sample does not reflect the chemical system in which the coronitic and/or symplectitic textures were developed. The composition for the *P–T* pseudosection modelling, which reflects the composition of the effectively reacting microdomains, was calculated from mineral compositions of sample NB6 (Table 1) and the stoichiometric coefficients of the balanced reaction (1a) (cf. Groppo *et al.*, 2007 for the description of the method). The following results were obtained in the CFMASH system (wt%): SiO_2 41.46; Al_2O_3 18.32; FeO 8.76; MgO 21.43; CaO 10.03. A small "albite" correction has been applied considering that little Na is present in plagioclase (see Table 1); therefore, very small Al_2O_3 and SiO_2 amounts have been subtracted from the bulk composition. Potassium was neglected as K-bearing phases are not involved in reaction (1a). All Fe has been considered as Fe^{2+}, because the Fe^{3+} content of the minerals involved in reaction (1a) is inferred to be negligible. The calculated composition for the reacting microdomain differs from the whole-rock composition (Brogioni *et al.*, 2007), being enriched in Al_2O_3 and CaO and depleted in FeO.

Pseudosections were calculated using the approach of Connolly (1990) and the internally consistent thermodynamic data set and the equation of state for H_2O by Holland & Powell (1998, revised 2002). The phases considered in the calculation were: olivine, plagioclase, quartz, orthopyroxene, clinopyroxene, spinel, garnet, amphibole, chlorite, zoisite, clinozoisite, lawsonite and talc. Solid-solution models and mixing parameters are those of Holland & Powell (1998) for olivine, spinel and garnet, Holland & Powell (1996) for pyroxene, Holland *et al.* (1998) for chlorite and Dale *et al.* (2005) for amphibole. An ideal solid-solution model was used for talc. H_2O was treated as a perfectly mobile component. The pseudosection has been calculated at aH_2O = 0.5 and at progressively increased water activity, in order to test the influence of aH_2O on the stability of the coronitic paragenesis. As aH_2O = 1 is unrealistic for the anhydrous high-*T* granulite facies assemblages of Opx_1-corona and Cpx_1 + Spl_1 symplectites (Touret, 1981), the pseudosection calculated at aH_2O = 0.5 is the first to be discussed.

Pseudosection of Fig. 4, calculated at 600–1000 °C, 1–15 kbar and aH_2O = 0.5, is dominated by di- (light grey) and tri-variant (intermediate grey) fields, with minor quadri-variant (dark grey) fields. The occurrence of garnet in most of the di-, tri- and quadri-variant fields at high-*P* conditions and the presence of chlorite in most of the fields at low temperatures are worthy of note. The systematic absence of garnet in our samples is therefore a pressure constraint, implying that at least the first part of the *P–T* path occurred at pressures lower than 8 kbar. According to the pseudosection, the mineral assemblage of Cpx_1 + Spl_1 symplectite plus coronitic orthopyroxene, which characterizes microdomains around olivine grains, could have been generated by near isobaric cooling at 7–8 kbar, when the rocks passed from the quadri-variant field Ol + Pl + (Opx) at 920 °C to the tri-variant field Opx + Cpx + Spl + (Pl) at lower temperatures (phases in brackets are present in very low modal amounts). Most of the isobaric paths connecting these two fields cross the tri-variant field Ol + Pl + (Opx) + (Spl), which differs from Ol + Pl + (Opx) for the presence of very small amount of Spl (< 1 vol.%; Fig. 5f), and thus it has no significant effects on the observed microstructures. Isomodes calculated for olivine, plagioclase, clino- and orthopyroxene and spinel (Fig. 5) indicate that: (i) the modal abundance of orthopyroxene in the quadri-variant field Ol + Pl + (Opx) (reactants) is negligible (< 3 vol.%), and (ii) the amount of reaction products (i.e. Opx + Cpx + Spl) abruptly increases at the transition between the two fields, confirming the discontinuous character for reaction (1a). Furthermore, the modal contents of clinopyroxene, spinel, orthopyroxene and plagioclase in the tri-variant Opx + Cpx + Spl + (Pl) field at 880 °C are 39.5, 19.5, 40 and 1 vol.%, respectively, resulting in a relative abundance of spinel in the Cpx_1 + Spl_1 symplectite of 33%, very similar to that estimated by image analysis (20–30%). The narrow Opx + Cpx + Spl + (Pl) three-variant field (see Fig. 4) also implies that the Opx + Cpx + Spl mineralogical assemblage was stable down to temperatures of 740 °C.

Microstructural relationships observed within the two symplectite types (patches and relics of the Cpx_1 + Spl_1 symplectite within the Am_1 + Spl_2 symplectite, see Fig. 3b–d) suggest that the Am_1 + Spl_2 symplectite formed after the Cpx_1 + Spl_1 symplectite. The formation of Am_1 + Spl_2 symplectite has been modelled by reaction (1b), which can be considered, together with reaction (1a), as an end-member of an infinity of plausible reactions. A second pseudosection has been calculated, at aH_2O = 0.5 (Fig. 6a), using the bulk composition resulting from

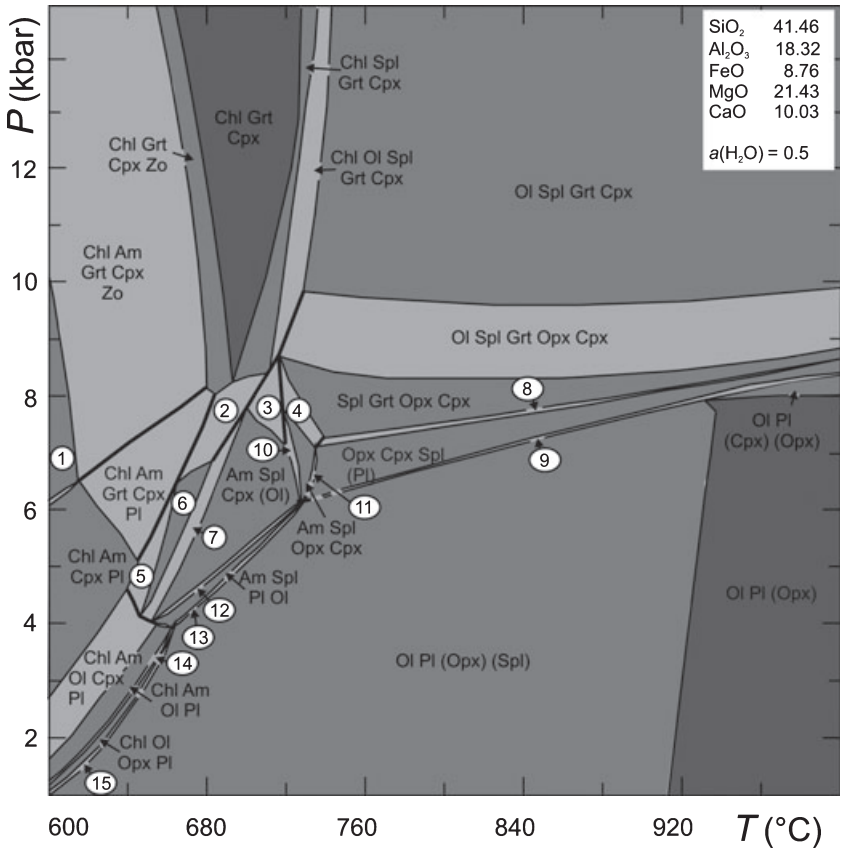

Fig. 4. *P–T* pseudosection modelled for the coronitic microdomain of El Arenal metagabbros, calculated in the CFMASH system at $aH_2O = 0.5$, using the bulk composition resulting from the balanced reaction (1a). Light grey, intermediate grey and dark grey fields are di-, tri- and quadri-variant fields, respectively. Phases in brackets are present in very low modal amount. Numbered assemblages are: (1) Chl Am Grt Zo; (2) Chl Am Spl Grt Cpx; (3) Am Spl Ol Grt Cpx; (4) Am Spl Grt Opx Cpx; (5) Chl Am Spl Cpx Pl; (6) Chl Am Spl Cpx; (7) Chl Am Ol Spl Cpx; (8) Spl Grt Opx Cpx Pl; (9) Ol Spl Opx Cpx Pl; (10) Am Ol Spl Opx Cpx; (11) Am Spl Opx Cpx Pl; (12) Am Ol Spl Cpx Pl; (13) Am Ol Spl Opx Pl; (14) Chl Am Ol Opx Pl; (15) Chl Ol Spl Opx Pl.

the balanced reaction (1b) (SiO_2 41.93; Al_2O_3 20.75; FeO 7.55; MgO 18.46; CaO 11.32 wt%); it does not significantly differ from the pseudosection of Fig. 4, except for some minor changes in the amphibole-bearing fields, at the lower temperature side of the diagram. If the water activity remained constant at $aH_2O = 0.5$ during the rock evolution, the pseudosection of Fig. 6a suggests that the $Am_1 + Spl_2$ symplectites formed at the transition between the Am-free field Opx + Cpx + Spl + (Pl) and the Am-bearing fields at < 730–740 °C. The $Am_1 + Spl_2$ symplectite formation thus required an isobaric cooling, or cooling during a slight decrease in pressure.

An alternative explanation may be that the $Am_1 + Spl_2$ symplectites were not related only to a temperature decrease, but also to local fluctuations in P_{H_2O}, as suggested by Godard & Martin (2000). The pseudosection of Fig. 6b has been calculated at $aH_2O = 1$, and shows that all the multivariant fields of Fig. 6a are shifted towards higher temperature as a consequence of the increase in aH_2O. As a result, the Am-bearing fields appear at < 790 °C, i.e. in a temperature range where only anhydrous assemblages are stable for a reduced water activity. Nevertheless, also at $aH_2O = 1$, $Cpx_1 + Spl_1$ symplectite and Opx_1 coronas are modelled to form prior to (at higher temperatures than) the $Am_1 + Spl_2$ symplectites, thus confirming microstructural observations.

THERMOBAROMETRY

Assuming that the orthopyroxene corona around olivine and the $Cpx_1 + Spl_1$ symplectite formed at the same time, we tried to estimate the temperature of their formation with the geothermometer based on the distribution of $Mg_2Si_2O_6$ between orthopyroxene and clinopyroxene (the two-pyroxene thermometer). Application of this geothermometer to coronitic orthopyroxene and symplectitic clinopyroxene from a single corona microdomain of sample NB6 (mineral data from Table 1) as calibrated by Wells (1977) yields a temperature estimate of 853 °C, while the calibrations by Wood & Banno (1973) and Brey & Köhler (1990) yielded 910 and 758 °C for a pressure of 8 kbar, respectively. The same calibrations applied to a coronitic microdomain from sample NB1 yielded temperatures in the range 810–923 °C. However, the calibration by Brey & Köhler (1990) tends to underestimate the equilibration temperature if applied to minerals with higher Fe content than those used for the actual calibration of the geothermometer. Moreover, these results should be considered with caution as the two pyroxenes used in the calculation are not in intimate intergrowth and could have failed to reach equilibrium at the microdomain scale.

The *P–T* conditions were also calculated with winTWQ version 2.10 (database 1.02 from Berman, 1988,

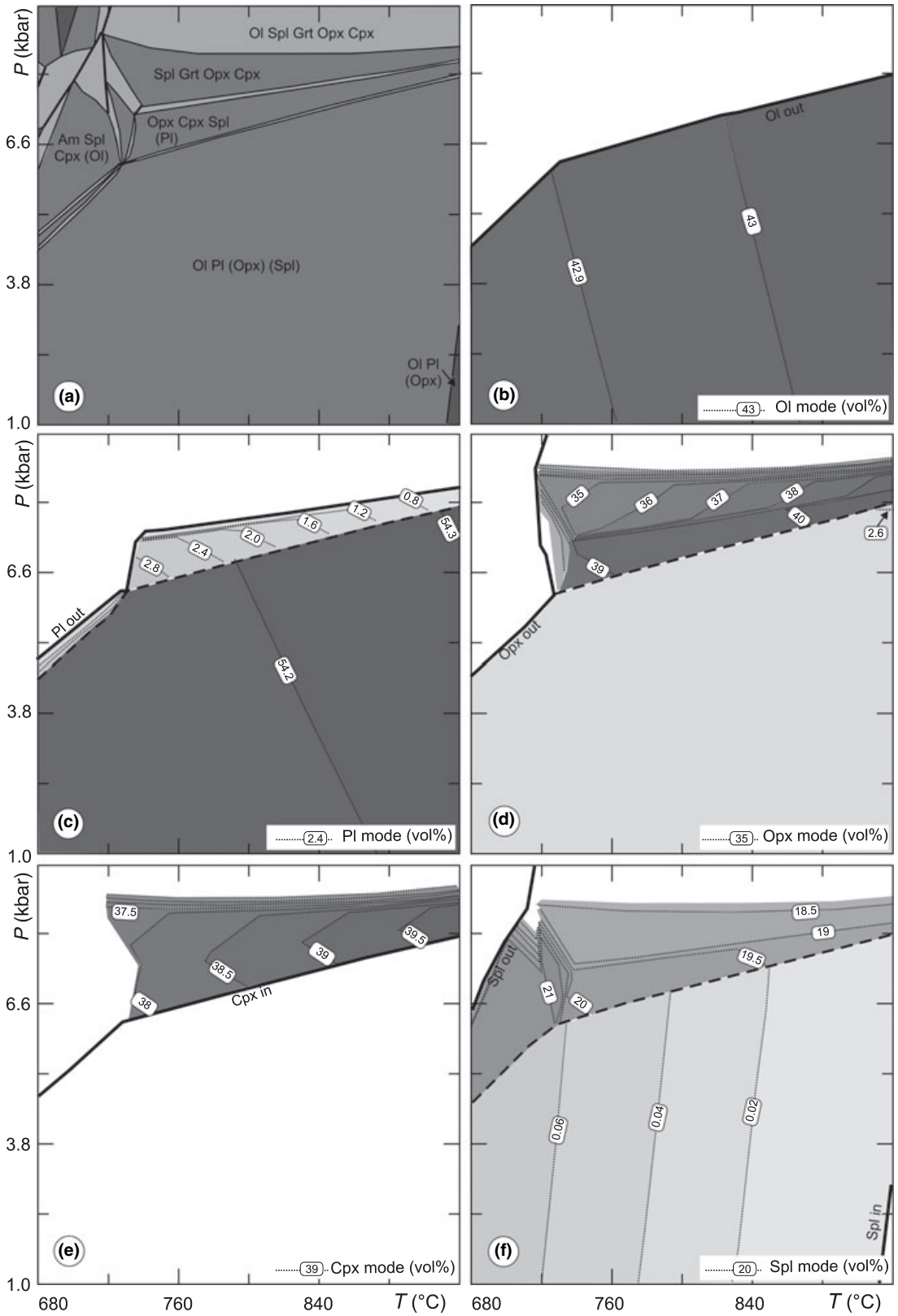

Fig. 5. Detail of the *P–T* pseudosection of Fig. 4 in the *P–T* interval 680–920 °C, 1.0–9.4 kbar (a), with isomodes (vol.%) for: olivine (b), plagioclase (c), orthopyroxene (d), clinopyroxene (e) and spinel (f). Progressively darker gray tones correspond to an increase in the modal amount of each phase.

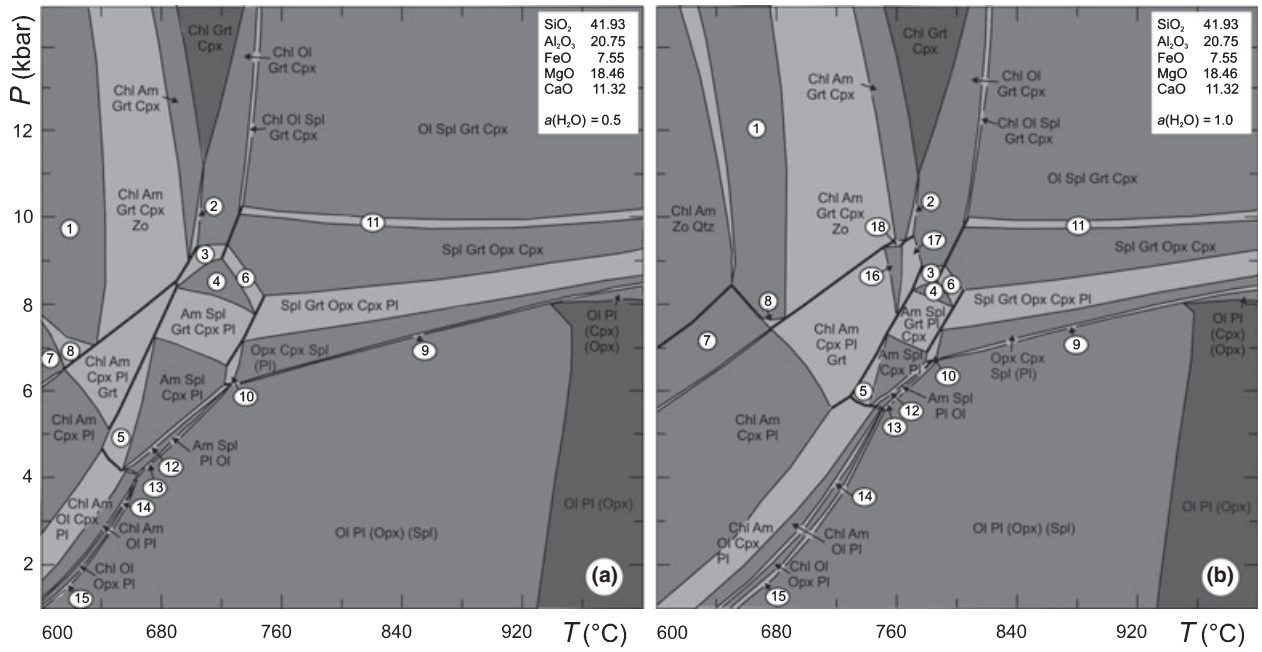

Fig. 6. *P–T* pseudosections modelled for the coronitic microdomain of El Arenal metagabbros, calculated in the CFMASH system at $aH_2O = 0.5$ (a) and $aH_2O = 1.0$ (b), using the bulk composition resulting from the balanced reaction (1b). Light grey, intermediate grey and dark grey fields are di-, tri- and quadri-variant fields, respectively. Numbered assemblages are: (1) Chl Am Grt Zo; (2) Chl Spl Grt Opx Zo; (3) Chl Am Spl Grt Opx; (4) Am Spl Grt Cpx; (5) Chl Am Spl Cpx Pl; (6) Am Spl Grt Opx Cpx; (7) Chl Am Ol Zo Pl; (8) Chl Am Grt Zo Pl; (9) Ol Spl Opx Cpx Pl; (10) Am Spl Opx Cpx Pl; (11) Ol Spl Grt Opx Cpx; (12) Am Ol Spl Cpx Pl; (13) Am Ol Spl Opx Pl; (14) Chl Am Ol Opx Pl; (15) Chl Ol Spl Opx Pl; (16) Chl Grt Cpx Pl; (17) Chl Spl Grt Cpx Pl; (18) Chl Grt Cpx Zo Pl.

1990) from the intersection of the following two independent equilibria:

$$6Fo + 2\ Tsch \rightarrow 4Spl + 5En + 4Di + 2H_2O$$

$$2Tsch \rightarrow 4An + En + 2Fo + 2H_2O$$

Solution models used in the calculation were those of Fuhrman & Lindsley (1988) for anorthite, Berman & Aranovich (1996) for olivine, Mäder *et al.* (1994) for amphibole, and ideal parameters for ortho- and clinopyroxene from Newton (1983). The average *P–T* conditions (906 °C and 7.8 kbar for sample NB6, 925 °C and 8.9 kbar for sample NB1, calculated for $aH_2O = 0.5$) from the intersection between the curves represent an estimate for the formation of the $Cpx_1 + Spl_1$ symplectite. In fact, the rocks should have passed, during cooling, above the intersection point of the two curves if the $Cpx_1 + Spl_1$ symplectite formed before the $Am_1 + Spl_2$-bearing one, as suggested by microtextural observations.

The temperature conditions of amphibole formation have been estimated by using the Holland & Blundy (1994) calibration of the Hbl + Pl thermometer applied to the composition of large pale-green amphibole porphyroblasts in mutual contact with metamorphic plagioclase Pl_1 (mineral data from Table 1). The re-equilibration temperatures are 712 and 706 °C for the edenite–tremolite equilibrium, at 5 and 10 kbar, respectively. The same geothermometer applied to symplectitic amphibole and Pl_1 yielded temperatures of 669–670 °C in the same pressure range.

The pressure estimate for amphibole formation has been obtained from the Al-in Hbl geobarometer calibrated by Hammarstrom & Zen (1986), Hollister *et al.* (1987) and Johnson & Rutherford (1989). Application of these calibrations to amphibole porphyroblast (Am_3) gives pressures of 6.9, 7.4 and 5.7 kbar (average = 6.6 kbar), respectively. The same calibrations applied to amphibole from the symplectite (Am_1) yields pressure conditions between 4.7 and 6.2 kbar.

P–T PATH AND GEOLOGICAL IMPLICATIONS

The *P–T* evolution suggested by microstructural relationships and modelled by pseudosection analysis is consistent with a nearly isobaric cooling, at $P \sim 7$–8 kbar, from ~920 °C down to < 790 °C (at $aH_2O = 1$) or < 740 °C (at $aH_2O = 0.5$) (Fig. 7). It is worthy to note that *P–T* conditions of 740–790 °C and 5.7–6.4 kbar reported by Hauzenberger *et al.* (2001) for the gneisses adjacent to the mafic rocks from the southern extreme of the Sierra de San Luis and those of 687–762 °C and 6.3–6.9 kbar reported by Delpino *et al.* (2007) for mafic mylonites and adjacent basement mylonites of the central sector of the Pringles

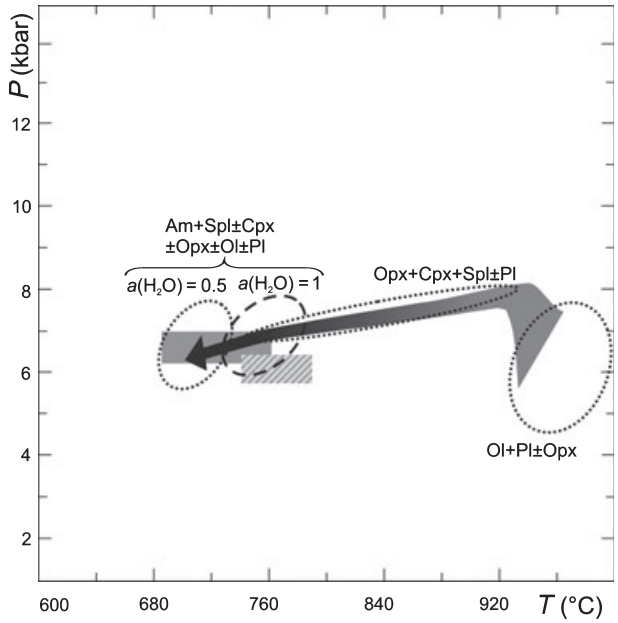

Fig. 7. *P–T* path for the El Arenal coronitic metagabbros as inferred from the modelled pseudosections of Figs 4 and 6. Dotted ellipses correspond to the stability fields of the igneous assemblage Ol + Pl ± Opx and coronitic assemblages Opx + Cpx + Spl ± Pl and Am + Spl ± Cpx ± Opx ± Ol ± Pl at reduced water activity (aH_2O = 0.5). Dashed ellipse corresponds to the stability field of the coronitic assemblage Am + Spl ± Cpx ± Opx ± Ol ± Pl at aH_2O = 1. The diagonally hatchured box refers to the *P–T* conditions estimated by Hauzenberger *et al.* (2001) for the gneisses adjacent to the mafic rocks of the Sierra de San Luis while the grey box represents *P–T* conditions for mafic mylonites and adjacent basement mylonites of the central sector of the Pringles Metamorphic Complex as reported by Delpino *et al.* (2007).

Metamorphic Complex are comparable with those inferred from the middle and the last part of the *P–T* path drawn in Fig. 7, respectively. After igneous crystallization, a cooling period is documented by the widespread occurrence of cloudy to platy Fe-oxides exsolved from the host igneous orthopyroxene. Although the thermobarometric results would have provided only indicative *P–T* conditions for the peak temperature, the orthopyroxene coronas and the Cpx_1 + Spl_1 symplectite probably began to form at *P–T* conditions of ~900 °C and 7–8 kbar in the granulite facies. Locally, pervasive growth of a hydrous, amphibole-bearing coronitic assemblage occurred at lower *P–T* conditions, typical of high-*T* amphibolite stage, ranging from 740 to 790 °C, depending on the water activity.

In summary, the coronitic microstructures and the *P–T* conditions reported above suggest that the El Arenal coronitic metagabbros underwent a complex evolution consisting of an igneous stage followed by, at least, two re-equilibration stages under *P–T* conditions of the granulite and high-*T* amphibolite facies. Finally, coexistence of chlorite and epidote suggests further, but not pervasive, re-equilibration under greenschist facies conditions.

The different stages of metamorphic re-crystallization through granulite, amphibolite and greenschist facies conditions point to a near isobaric cooling, through a *P–T* path similar to those followed by gabbroic rocks emplaced in the lower crust and progressively cooled down. A similar interpretation has been proposed by Mogessie *et al.* (2000) for the mafic–ultramafic rocks from Las Aguilas, in the southern extreme of the mafic belt. The thermal effect of mafic–ultramafic bodies intruded into an older crystalline basement resulted in granulite facies metamorphism of the basement in contact with the intrusive rocks, whereas the mafic–ultramafic rocks re-equilibrated to high-grade metamorphic temperature in the range 700–800 °C (Mogessie *et al.*, 2000).

Granulitic *P–T* conditions deriving from post-magmatic cooling, have also been proposed by Baldo *et al.* (1999) for granulite facies metamorphism (690 ± 90 °C and 4.1 ± 0.4 kbar) of coronitic metagabbros from the Sierra de Valle Fértil (Sierras Pampeanas Occidentales), while *P–T* conditions obtained from mafic mylonites and adjacent basement mylonites (687–762 °C, 6.3–6.9 kbar) in the Pringles Metamorphic Complex of the Sierras Pampeanas of San Luis indicate conditions of deformation in the upper amphibolite transitional to granulite facies at medium pressure (Delpino *et al.*, 2007). Amphibolitization in the El Arenal coronitic metagabbros resulted from the regional metamorphism ascribed to the main phase of the Famatinian orogeny. Amphibolitization was triggered by the thermal supply provided by the igneous rocks and favoured by the consequent dehydration of the adjacent metasedimentary rocks. Finally, the rocks experienced greenschist facies metamorphism during the final part of the counterclockwise *P–T* path.

ACKNOWLEDGEMENTS

We are grateful to G. Godard (Université Paris 7) and H. M. Lang (West Virginia University) for their helpful comments and constructive criticism. Financial support was provided by Progetti di Ricerca Locale, Università di Cagliari funds to M. Franceschelli.

REFERENCES

Baldo, E. G. A., Murra, J. A., Casquet, C., Galindo, C. & Saavedra, J., 1999. El gabro coronítico de la Sierra de Valle Fértil, Sierras Pampeanas Argentina: condiciones *P-T* de la etapa coronítica. *Boletín de la Sociedad Española de Mineralogía*, **22-A,** 17–18.

Berman, R. G., 1988. Internally-consistent thermodynamic data for minerals in the system Na_2O-K_2O-CaO-MgO-FeO-Fe_2O_3-Al_2O_3-SiO_2-TiO_2-H_2O-CO_2. *Journal of Petrology*, **29,** 445–522.

Berman, R. G., 1990. Mixing properties of Ca-Mg-Fe-Mn garnets. *American Mineralogist*, **75,** 328–344.

Berman, R. G. & Aranovich, L. Y., 1996. Optimized standard state and solution properties of minerals I. Model calibration for olivine, orthopyroxene, cordierite, garnet and ilmenite in the system FeO-MgO-CaO-Al_2O_3-TiO_2-SiO_2. *Contributions to Mineralogy and Petrology*, **126,** 1–24.

Brey, G. P. & Köhler, T., 1990. Geothermobarometry in four-phase lherzolites. II. New thermobarometers, and practical assessment of existing thermobarometers. *Journal of Petrology*, **31,** 1353–1378.

Brogioni, N., 1994. Petrología de la faja de rocas máficas y ultramáficas de la Sierra de San Luis, Argentina. *7 Congreso Geológico Chileno, Actas*, **2,** 967–971.

Brogioni, N., 2001. Petrología de los cuerpos Virorco y El Fierro, faja máfica-ultramáfica del borde oriental de la Sierra de San Luis. *Revista de la Asociación Geológica Argentina*, **56,** 535–547.

Brogioni, N., Cruciani, G., Franceschelli, M. & Vaselli, O., 2007. Evolución metamórfica de las melagabronoritas coroníticas de El Arenal, faja máfica-ultramáfica El Destino-Las Aguilas, Sierra de San Luis. *Revista de la Asociación Geológica Argentina*, **62,** 13–24.

Bucher, K. & Frey, M., 2002. *Petrogenesis of Metamorphic Rocks*, 7th edn. Springer-Verlag, Berlin, 341 pp.

Burnham, C. W., Holloway, J. R. & Davis, N. F., 1969. Thermodynamic properties of water to 1,000 °C and 10,000 bars. *Geological Society of America Special Paper*, **132,** 96 pp.

Connolly, J. A. D., 1990. Multivariable phase diagrams: an algorithm based on generalized thermodynamics. *American Journal of Science*, **290,** 666–718.

Dale, J., Powell, R., White, R. W., Elmer, F. L. & Holland, T. J. B., 2005. A thermodynamic model for Ca–Na clinoamphiboles in Na_2O–CaO–FeO–MgO–Al_2O_3–SiO_2–H_2O–O for petrological calculations. *Journal of Metamorphic Geology*, **23,** 771–791.

Delpino, S. H., Bjerg, E. A., Ferracutti, G. R. & Mogessie, A., 2007. Counterclockwise tectonometamorphic evolution of the Pringles Metamorphic Complex, Sierras Pampeanas of San Luis (Argentina). *Journal of South American Earth Sciences*, **23,** 147–175.

Ferracutti, G., Bjerg, E. & Mogessie, A., 2007. Metales base y preciosos en Las Aguilas, sierra de San Luis: mineralogía, génesis y evolución. *Revista de la Asociación Geológica Argentina*, **62,** 329–488.

Fisher, G. W., 1989. Matrix analysis of metamorphic mineral assemblages and reactions. *Contributions to Mineralogy and Petrology*, **102,** 69–77.

Fuhrman, M. L. & Lindsley, D. H., 1988. Ternary-feldspar modeling and thermometry. *American Mineralogist*, **73,** 201–215.

Godard, G. & Martin, S., 2000. Petrogenesis of kelyphites in garnet peridotites: a case study from the Ulten zone, Italian Alps. *Journal of Geodynamics*, **30,** 117–145.

González Bonorino, F., 1961. Petrología de algunos cuerpos básicos de San Luis y las granulitas asociadas. *Revista de la Asociación Geológica Argentina*, **16,** 61–106.

von Gosen, W. & Prozzi, C., 1998. Structural evolution of the Sierra de San Luis (Eastern Sierras Pampeanas, Argentina): implications for the Proto-Andean margin of Gondwana. In: *The Proto-Andean Margin of Gondwana, Special Publications 142* (eds Pankhurst, R. J. & Rapela, C.), pp. 235–258. Geological Society, London.

Groppo, C., Lombardo, B., Castelli, D. & Compagnoni, R., 2007. Exhumation history of the UHPM Brossasco-Isasca Unit, Dora-Maira Massif, as inferred from a phengite-amphibole eclogite. *International Geology Review*, **49,** 142–168.

Hammarstrom, J. M. & Zen, E., 1986. Aluminium in hornblende: an empirical igneous geobarometer. *American Mineralogist*, **71,** 1297–1313.

Hauzenberger, C. A., Mogessie, A., Hoinkes, G. *et al.*, 2001. Metamorphic evolution of the Sierras de San Luis, Argentina: granulite facies metamorphism related to mafic intrusions. *Mineralogy and Petrology*, **71,** 95–126.

Helgeson, H. C., Delaney, J. M., Nesbitt, H. W. & Bird, D. K., 1978. Summary and critique of the thermodynamic properties of rock-forming minerals. *American Journal of Science*, **278A,** 229 pp.

Holland, T. J. B. & Blundy, J. D., 1994. Non-ideal interactions in calcic amphiboles and their bearing on amphibole-plagioclase thermometry. *Contributions to Mineralogy and Petrology*, **116,** 433–447.

Holland, T. J. B. & Powell, R., 1996. Thermodynamics of order-disorder in minerals, 2. Symmetric formalism applied to solid solutions. *American Mineralogist*, **81,** 1425–1437.

Holland, T. J. B. & Powell, R., 1998. An internally consistent thermodynamic data set for phases of petrologic interest. *Journal of Metamorphic Geology*, **16,** 309–343.

Holland, T., Baker, J. & Powell, R., 1998. Mixing properties and activity-composition relationships of chlorites in the system MgO-FeO-Al_2O_3-SiO_2-H_2O. *European Journal of Mineralogy*, **10,** 395–406.

Hollister, L. S., Grissom, G. C., Peters, E. K., Stowell, H. H. & Sisson, V. B., 1987. Confirmation of the empirical correlation of aluminium in hornblende with pressure of solidification of calc-alkaline plutons. *American Mineralogist*, **72,** 231–239.

Ikeda, T., Nishiyama, T., Yamada, S. & Yanagi, T., 2007. Microstructures of olivine-plagioclase corona in meta-ultramafic rocks from Sefuri Mountains, NW Kyushu, Japan. *Lithos*, **97,** 289–306.

Johnson, M. C. & Rutherford, M. J., 1989. Experimental calibration of the aluminum-in-hornblende geobarometer with application to Long Valley Caldera (California) volcanic rocks. *Geology*, **17,** 837–841.

Kretz, R., 1983. Symbols for rock forming minerals. *American Mineralogist*, **68,** 277–279.

Lang, H. M., Wachter, A. J., Peterson, V. L. & Ryan, J. G., 2004. Coexisting clinopyroxene/spinel and amphibole/spinel symplectites in metatroctolites from the Buck Creek ultramafic body, North Carolina Blue Ridge. *American Mineralogist*, **89,** 20–30.

Leake, B. E., Woolley, A. R., Arps, C. E. S. *et al.*, 1997. Nomenclature of amphiboles: report of the subcommittee on amphiboles of the International Mineralogical Association, commission on new minerals and mineral names. *Canadian Mineralogist*, **35,** 219–246.

Mäder, U. K., Percival, J. A. & Berman, R. G., 1994. Thermobarometry of garnet–clinopyroxene-hornblende granulites from the Kapuskasing structural zone. *Canadian Journal of Earth Sciences*, **31,** 1134–1145.

Mall, A. P. & Sharma, R. S., 1988. Coronas in olivine metagabbros from the Proterozoic Chotanagpur terrain at Mathurapur, Bihar, India. *Lithos*, **21,** 291–300.

Malvicini, L. & Brogioni, N., 1996. Las Aguilas Este Deposit: Shear zone hosted hydrothermal Cu-Ni sulfide and platinum-group elements mineralization in the mafic-ultramafic complex of San Luis Range, Argentina. In: *Geology and Ore Deposits of the American Cordillera* (eds Coyner, A. & Fahey, P.), pp. 1475–1485. Geological Society of Nevada Symposium Proceedings, Reno/Sparks, NV, USA.

Mogessie, A., Hauzenberger, Ch. A., Hoinkes, G. *et al.*, 2000. Genesis of platinum-group minerals in the Las Aguilas mafic-ultramafic rocks, San Luis Province, Argentina: textural, chemical and mineralogical evidence. *Mineralogy and Petrology*, **68,** 85–114.

Newton, R. C., 1983. Geobarometry of high-grade metamorphic rocks. *American Journal of Science*, **283,** 1–28.

Ortiz Suárez, A., Prozzi, C. & Llambías, E., 1992. Geología de la parte sur de la Sierra de San Luis y granitoides asociados, Argentina. *Estudios Geológicos*, **48,** 269–277.

Pankhurst, R. J. & Rapela, C. W., 1998. The proto-Andean margin of Gondwana: an introduction. In: *The Proto-Andean Margin of Gondwana, Special Publications 142* (eds Pankhurst, R. J. & Rapela, C.), pp. 1–9. Geological Society, London.

Sato, A., González, P. & Llambías, E., 2003. Evolución del orógeno Famatiniano en la Sierra de San Luis: magmatismo

de arco, deformación y metamorfismo de bajo a alto grado. *Revista de la Asociación Geológica Argentina*, **58,** 487–504.

Sims, J. P., Stuart-Smith, P., Lyons, P. & Skirrow, R. G., 1997a. *Informe geológico y metalogenético de las Sierras de San Luis y Comechingones, Provincias de San Luis y Córdoba*. Mapeo geocientífico de las Sierras Pampeanas, Proyecto de Cooperación Argentino-Australiano, Servicio Geológico Minero Argentino, Buenos Aires, 148 pp. (Inédito).

Sims, J. P., Stuart-Smith, P., Lyons, P. & Skirrow, R., 1997b. *Report on 1:250.000 scale geological and metallogenic maps Sierra de San Luis and Comechingones, Provinces of San Luis and Córdoba*. Unpublished Report, Geoscientific Mapping of the Sierras Pampeanas Argentine-Australian Cooperative Project.

Sims, J. P., Ireland, T., Camacho, A. *et al.*, 1998. U-Pb, Th-Pb and Ar-Ar geochronology from the southern Sierras Pampeanas, Argentina: implications for the Palaeozoic tectonic evolution of the western Gondwana margin. In: *The Proto-Andean Margin of Gondwana, Special Publications 142* (eds Pankhurst, R. J. & Rapela, C.), pp. 259–281. Geological Society, London.

Torres-Roldan, R. L., Garcia-Casco, A. & Garcia-Sanchez, P. A., 2000. CSpace: an integrated workplace for the graphical and algebraic analysis of phase assemblages on 32-bit wintel platforms. *Computers & Geosciences*, **26,** 779–793.

Touret, J., 1981. Fluid inclusions in high grade metamorphic rocks. In: *Short Course in fluid inclusions: applications to petrology, 6* (eds Hollister, L. S. & Crawford, M. L.), pp. 182–208. Mineralogical Association of Canada, Calgary.

Wells, P. R. A., 1977. Pyroxene thermometry in simple and complex systems. *Contributions to Mineralogy and Petrology*, **62,** 129–139.

Wood, B. J. & Banno, S., 1973. Garnet-orthopyroxene and garnet-clinopyroxene relationships in simple and complex systems. *Contributions to Mineralogy and Petrology*, **42,** 109–124.

Received 4 December 2007; revision accepted 19 May 2008

APPENDIX

Matrix of residuals for reaction (1a):

	Ol	Pl	Spl	Opx	Cpx
SiO_2	0.0042	0.0023	−0.0020	−0.0022	−0.0024
$AlO_{1.5}$	−0.0056	−0.0031	0.0027	0.0029	0.0032
CaO	0.0009	0.0005	−0.0004	−0.0005	−0.0005
$NaO_{0.5}$	−0.0017	−0.0009	0.0008	0.0009	0.0010
MgO	−0.0165	−0.0091	0.0080	0.0085	0.0095
FeO	0.0524	0.0288	−0.0253	−0.0270	−0.0302

Matrix of residuals for reaction (1b):

	Ol	Pl	Spl	Am	H_2O
SiO_2	0.0028	0.0021	−0.0010	−0.0010	0.0011
$AlO_{1.5}$	−0.0028	−0.0020	0.0010	0.0010	−0.0010
CaO	−0.0076	−0.0055	0.0028	0.0028	−0.0028
$NaO_{0.5}$	0.0767	0.0553	−0.0282	−0.0281	0.0286
MgO	−0.0182	−0.0132	0.0067	0.0067	−0.0068
FeO	0.0485	0.0350	−0.0178	−0.0178	0.0181
H_2O	−0.0032	−0.0023	0.0012	0.0012	−0.0012

Matrix of residuals for reaction (2):

	Pl	Spl	Opx	Am	H_2O
SiO_2	−0.0395	0.0115	−0.0777	0.0327	−0.0358
$AlO_{1.5}$	−0.0105	0.0031	−0.0207	0.0087	−0.0095
CaO	0.0875	−0.0254	0.1719	−0.0725	0.0793
$NaO_{0.5}$	0.0531	−0.0154	0.1043	−0.0440	0.0481
MgO	0.0297	−0.0086	0.0584	−0.0246	0.0269
FeO	0.0133	−0.0039	0.0261	−0.0110	0.0121
H_2O	−0.0121	0.0035	−0.0238	0.0100	−0.0110

Matrix of residuals for reaction (3):

	Opx	Am	Cpx	H_2O
SiO_2	0.0297	−0.0170	0.0362	0.0176
$AlO_{1.5}$	0.0261	−0.0150	0.0319	0.0155
CaO	−0.0417	0.0240	−0.0510	−0.0248
$NaO_{0.5}$	0.0248	−0.0142	0.0303	0.0147
MgO	−0.0276	0.0158	−0.0337	−0.0164
FeO	−0.0763	0.0438	−0.0932	−0.0453
H_2O	−0.0063	0.0036	−0.0077	−0.0037